Malaysian Journal of Analytical Sciences (MJAS)
Published by Malaysian Analytical Sciences Society

ENHANCED CO_2 CAPTURE PERFORMANCE OF TITANIUM-MODIFIED SBA-15: SYNTHESIS, CHARACTERIZATION, AND FIXED-BED COLUMN ADSORPTION STUDY

(Prestasi Penjerapan CO_2 yang Dipertingkatkan bagi SBA-15 Terubahsuai Titanium: Sintesis, Pencirian dan Kajian Penjerapan Turus Lapisan Tetap)

Shalini Mahendran[1], Noorfatimah Yahaya[2], Bassim H. Hameed[3], Dai Viet N. Vo[4], Abdelkader Quakouak[5], Norikazu Nishiyama[6], and Azam Taufik Mohd Din[1*]

[1]*School of Chemical Engineering, Engineering Campus, Universiti Sains Malaysia, 14300 Nibong Tebal, Pulau Pinang, Malaysia*
[2]*Integrative Medicine Cluster, Advanced Medical and Dental Institute (AMDI), Universiti Sains Malaysia, 13200 Kepala Batas, Pulau Pinang, Malaysia*
[3]*Department of Chemical Engineering, College of Engineering, Qatar University, P.O. Box: 2713, Doha, Qatar,*
[4]*Institue of Environmental Technology and Sustainable Development, Nguyen Tat Thanh University, 298-300A Nguyen Tat Thanh, District 4, Ho Chi Minh City, 755414, Viet Nam*
[5]*Hydraulic and Civil Engineering Department, University of El Qued, PO Box 789, El Qued, 39000, Algeria*
[6]*Division of Chemical Engineering, Graduate School of Engineering Science, Osaka University, 1-3 Machikaneyama, Toyonaka, Osaka 560-8531, Japan*

[*]*Corresponding author: chazam@usm.my*

Received: 17 July 2024; Accepted: 11 September 2024; Published: 29 December 2024

Abstract

Global warming is widely recognized as one of humanity's most pressing challenges. It is primarily driven by the greenhouse effect, whereby greenhouse gases, predominantly CO_2, trap heat close to the surface of the Earth. The accumulation of CO2 in high concentrations can have various negative effects on the environment, such as global warming, ocean acidification and reduced crop yields. Therefore, it is crucial to mitigate CO_2 emissions by employing carbon capture techniques. In this study, Pluronic P123 (a non-ionic surfactant) and TEOS (a silica source) were utilized in a sol-gel process to fabricate an ordered mesoporous silica, known as SBA-15, as catalyzed by hydrochloric acid (HCl). Subsequently, the synthesized adsorbent was modified with titanium (IV) isopropoxide (TIP) to enhance its physicochemical properties and adsorption capacity, which resulted in the Ti-SBA-15. This modified adsorbent was then evaluated using a fixed-bed column adsorption system to investigate the impacts of different factors, namely CO_2 adsorption temperature, inlet gas concentration, adsorbent loading, and gas flow rate. Physicochemical analyses, such as scanning electron microscope (SEM), energy dispersive X-ray spectroscopy (EDX), X-ray diffraction analysis (XRD), Fourier transform infrared (FTIR), transmission electron microscopy (TEM), BET surface analysis, X-ray photoelectron spectroscopy (XPS), and atomic force microscopy (AFM) were conducted on the Ti-SBA-15. Experimental results were interpreted using the pseudo-first-order and pseudo-second-order kinetics, as well as the Avrami model, with the Avrami model showing the best fit. The Thomas and Yoon-Nelson models effectively predicted the CO_2 adsorption performance in the fixed-bed column. Thermodynamic modeling confirmed the exothermic and positively spontaneous nature of the reaction. Overall, Ti-SBA-15

demonstrated a promising ability as a low-cost, high-capacity CO_2 capture adsorbent, while maintaining its adsorption efficiency, even through multiple cycles of reuse.

Keywords: Ordered mesoporous silica, Ti-SBA-15, CO_2 adsorption, fixed-bed column adsorption, kinetics modeling

Abstrak

Pemanasan global diiktiraf secara meluas sebagai salah satu cabaran paling mendesak umat manusia. Ia terutamanya didorong oleh kesan rumah hijau, di mana gas rumah hijau, kebanyakannya CO_2, memerangkap haba dekat dengan permukaan Bumi. Pengumpulan CO_2 dalam kepekatan tinggi boleh menyebabkan kesan-kesan negatif ke atas persekitaran seperti pemanasan global, asidifikasi lautan dan mengurangkan hasil tanaman. Oleh itu, adalah penting untuk mengurangkan pelepasan CO_2 dengan menggunakan teknik penangkapan karbon. Dalam kajian ini, Pluronic P123 (surfaktan bukan ionik) dan TEOS (sumber silika) telah digunakan dalam proses sol-gel untuk menghasilkan silika mesoliang tersusun, dikenali sebagai SBA-15, seperti yang dimangkinkan oleh asid hidroklorik (HCl). Selepas itu, penjerap tersintesis telah diubah suai dengan titanium (IV) isopropoksida (TIP) untuk meningkatkan sifat fizikokimia dan kapasiti penjerapannya, yang menghasilkan Ti-SBA-15. Bahan penjerap yang diubah suai ini kemudiannya dinilai menggunakan sistem penjerapan turus lapisan tetap untuk menyiasat kesan faktor yang berbeza, iaitu suhu penjerapan CO_2, kepekatan gas masuk, pemuatan penjerap, dan kadar aliran gas. Analisis fizikokimia, seperti pengimbasan mikroskop elektron (SEM), spektroskopi sinar-X penyebaran tenaga (EDX), analisis pembelauan sinar-X (XRD), inframerah transformasi Fourier (FTIR), mikroskop elektron penghantaran (TEM), analisis permukaan BET, spektroskopi fotoelektron sinar-X (XPS), dan mikroskopi daya atom (AFM) telah dijalankan pada Ti-SBA-15. Keputusan eksperimen telah ditafsirkan menggunakan kinetik pseudo-tertib pertama dan pseudo-kedua, serta model Avrami, dengan model Avrami menunjukkan kesesuaian terbaik. Model Thomas dan Yoon-Nelson secara berkesan meramalkan prestasi penjerapan CO_2 dalam turus lapisan tetap. Pemodelan termodinamik mengesahkan sifat eksotermik dan spontan positif tindak balas. Secara keseluruhan, Ti-SBA-15 menunjukkan keupayaan yang menjanjikan sebagai penjerap tangkapan CO_2 berkos rendah dan berkapasiti tinggi, sambil mengekalkan kecekapan penjerapannya, walaupun melalui pelbagai kitaran penggunaan semula.

Kata kunci: Silika mesoliang tersusun, Ti-SBA-15, penjerapan CO_2, penjerapan turus lapisan tetap, pemodelan kinetik

Introduction

The escalating levels of carbon dioxide (CO_2) emissions, primarily attributed to industrial activities, fossil fuel combustion, and land-use changes constitute a significant contributor to global climate change. In 2019, global CO_2 emissions from fossil fuel combustion and industrial processes reached an estimated 36.8 billion metric tons, representing a 62% increase since 1990 [1]. CO_2 emissions are a byproduct of numerous human activities, including energy production, transportation, industrial processes, and deforestation. These emissions are contributing to the greenhouse effect, leading to global warming and climate change [2]. Without significant and sustained efforts to reduce its emissions, global temperatures are projected to rise by 3 to 4 °C by the end of the century, with catastrophic consequences for ecosystems, economies, and human well-being [3]. Therefore, urgent actions are needed to accelerate the transition to a low-carbon economy and mitigate the impacts of climate change on a global scale.

Numerous existing conventions, policies, and initiatives have been established at both the international and national levels to address the challenges of climate change and mitigate CO_2 emissions. The Paris Agreement, as adopted in 2015 under the United Nations Framework Convention on Climate Change (UNFCCC), represents a landmark international treaty aimed at limiting global warming to well below 2 °C above pre-industrial levels, with efforts to limit the temperature increase to 1.5 °C. This agreement outlines national commitments to reducing greenhouse gas emissions, increasing climate resilience, and providing financial support to developing countries [4]. However, the success of these policies and conventions in effectively mitigating CO_2 emissions remains a subject of debate. While the Paris Agreement has been hailed as a significant step forward in international climate action, critics argue that the voluntary nature of the agreement and the lack of binding enforcement mechanisms are undermining its effectiveness. Some countries have failed to meet their emission reduction targets, and political challenges

have hindered progress on key issues, such as climate finance and technology transfer [5].

As concerns regarding climate change intensify, there is a pressing need for effective strategies to mitigate CO_2 emissions and reduce their adverse environmental impact. Among the various approaches, CO_2 capture and storage technologies have emerged as critical components in the fight against climate change [6]. This necessitates the exploration and development of advanced materials that are capable of efficiently capturing and storing CO_2 from various emission sources. To mitigate CO_2 emissions, several strategies have been proposed, including energy efficiency improvements, increased adoption of renewable energy sources, carbon capture and storage (CCS) technologies, and afforestation efforts [7]. Among these, CCS technologies hold promise for capturing CO_2 directly from industrial sources, such as power plants and cement factories before it is released into the atmosphere. The captured CO_2 can then be transported and stored underground in geological formations, preventing its release into the atmosphere and mitigating its impact on climate change [8].

Adsorbent materials play a crucial role in CO_2 capture technologies, as they are responsible for selectively capturing CO_2 molecules from gas streams. Several types of adsorbents have been investigated for CO_2 capture applications, each with its advantages and limitations. Activated carbons are widely used due to their high surface area and porosity, but they often lack the necessary selectivity for CO_2 [9]. Metal-organic frameworks (MOFs) offer tunable pore structures and high CO_2 adsorption capacities but may suffer from stability issues under practical operating conditions [10]. Zeolites are known for their excellent thermal stability and selectivity but may have limited CO_2 adsorption capacities [11]. Mesoporous silica materials such as SBA-15 exhibit ordered pore structures and high surface areas, making them promising candidates for CO_2 capture applications [12].

SBA-15 is a type of ordered mesoporous silica with hexagonally arranged cylindrical pores, large surface areas, and high pore volumes [13]. These structural characteristics make SBA-15 attractive for CO_2 capture applications. However, SBA-15 also possesses inherent limitations that can affect its CO_2 adsorption performance. Its hydrophobic nature and weak interaction with CO_2 molecules can limit its adsorption capacity, particularly at low temperatures and under humid conditions. Additionally, the presence of silanol groups on the silica surface may lead to competitive adsorption of moisture and other gases, reducing the efficiency of CO_2 capture [14].

To address the limitations of SBA-15 and improve its CO_2 adsorption performance, researchers have explored various modification strategies. One promising approach involved the functionalization of SBA-15 with metal oxides such as titanium dioxide (TiO_2) [15]. Titanium (IV) isopropoxide (TIP) serves as a precursor for TiO_2 and can be incorporated into the SBA-15 framework through co-condensation [16] or post-synthesis grafting methods [17]. The addition of titanium species introduces Lewis acid sites on the silica surface, which can enhance the interaction with CO_2 molecules through coordination bonds, thereby improving the adsorption capacity and selectivity of the material [18]. Furthermore, titanium modification can modify the surface chemistry of SBA-15, rendering it more hydrophilic and less prone to moisture interference, thereby enhancing its stability and performance under humid conditions [19].

In summary, the development of advanced adsorbent materials for CO_2 capture is essential for mitigating greenhouse gas emissions and combating climate change. Titanium modification of ordered mesoporous silica such as SBA-15 represents a promising approach to enhance CO_2 adsorption performance by addressing the inherent limitations of the material. Further research efforts are warranted to optimize the synthesis methods, investigate structure-property relationships, and evaluate the practical applicability of titanium-modified SBA-15 for large-scale CO_2 capture applications

Materials and Methods

Materials

Pluronic P123, an amphiphilic triblock copolymer, and tetraethyl orthosilicate (TEOS) sourced from Sigma-

Aldrich were used as received. Hydrochloric acid (37%) from Sigma-Aldrich was also utilized. Distilled water was the solvent for all experiments. N_2 and CO_2 gases, both 99% pure, were supplied by Air Products Malaysia Sdn. Bhd. and served as the carrier gas and adsorbate, respectively, for the adsorption studies.

Synthesis of SBA-15

Initially, 150 mL of 2.5 M HCl was used to dissolve 5 g of Pluronic P123 and the solution was stirred until it turned colorless. Subsequently, 9.67 g of TEOS was introduced to the solution after the complete dissolution of Pluronic P123, resulting in the formation of a white solution after 2h of stirring at 40 °C. This solution was then transferred to a water bath shaker and aged for 48h until a white precipitate emerged. This precipitate was filtered and washed continuously with distilled water. The residue underwent natural drying at room temperature before being subjected to calcination at 550 °C for 4h at a heating rate of 5 °C/min to eliminate the P123-TEOS template. Following calcination, the precipitate was allowed to cool to room temperature, filtered again, and washed continuously with distilled water. To obtain SBA-15, the calcined precipitate was dried in an oven for 12h [20]. Figure 1 shows the schematic diagram of the synthesis of the SBA-15 adsorbent.

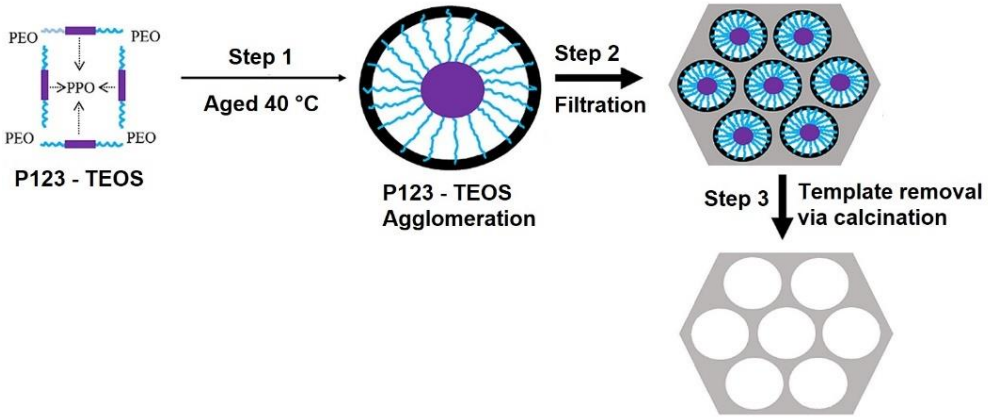

Figure 1. Schematic diagram of the synthesis of SBA-15 [21]

Functionalization of titanium on SBA-15

Approximately 1 g of SBA-15, as prepared in the procedure, was combined with a mixture of 10 mL of ethanol and 0.5 g of titanium (IV) isopropoxide (TIP). This mixture was stirred at room temperature for 1h. Subsequently, this mixture was allowed to dry for 12h at room temperature before being transferred to an oven for complete drying at 100 °C for 10h [16]. After cooling, the prepared adsorbent was ready for CO_2 adsorption. This process was repeated using different ratios of TIP to adsorbent to achieve a modified adsorbent with optimal adsorption capacity. Figure 2**Error! Reference source not found.** shows the schematic diagram of the synthesis of the titanium-modified SBA-15 (Ti-SBA-15) adsorbent.

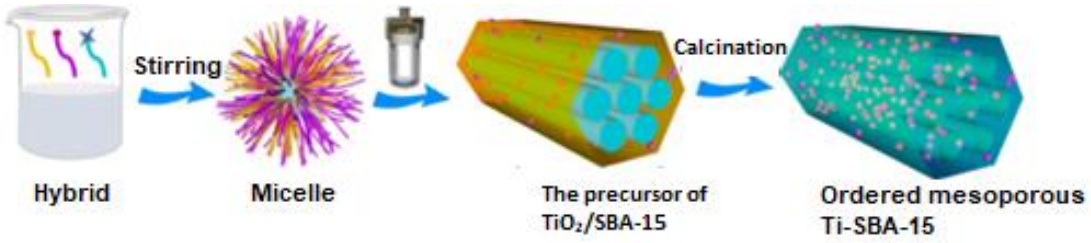

Figure 2. Schematic diagram of the synthesis of Ti-SBA-15 [22]

Characterization of adsorbent

The morphology of the synthesized Ti-SBA-15 was examined using a scanning electron microscope (SEM FEI Quanta 450 FEG), while the textural features were captured using a transmission electron microscope (Philips TEM C12, The Netherlands). The elemental composition of the Ti-SBA-15 was determined using an energy dispersive X-ray (EDX Perkin-Elmer2400 Series II CHNS/O). Fourier-transform infrared spectroscopy (FTIR) analysis was conducted using a Thermo Scientific Nicolet iS10 spectrometer to identify the surface functional groups, chemical bonds, and structure of the adsorbent. FTIR spectra were acquired by pelletizing the material in potassium bromide (KBr) within the range of 4000 to 400 cm^{-1}. The surface area and porosity of the adsorbent were assessed using the Brunauer-Emmett-Teller (BET) method with a Micromeritics ASAP 2020 analyzer that employed physical N_2 adsorption at 77 K. The average pore size distribution and total pore volume were determined using the Barrett-Joyner-Halenda and t-plot methods, while the surface area was calculated using the BET equation. Small-angle X-ray diffraction with 2θ ranging from 0.5° to 2.5° was utilized to observe the ordered hexagonal mesoporous structures of the samples. X-ray photoelectron spectroscopy (XPS) analysis was carried out using the Kratos Ultra2 Shimadzu X-ray photoelectron spectrometer. Atomic force microscopy (AFM) pictures were taken using the Veeco Instruments MMAFM-2. The adsorbent materials were prepared by homogenizing and finely powdering them in pure ethanol using an ultrasonic bath. Then, they were applied onto freshly exfoliated mica sheets for examination in tapping mode using silicon cantilevers with a 4 nm tip radius.

Adsorption and desorption experiments

The adsorption performance of the synthesized samples was tested using a fixed-bed reactor under different conditions, namely different temperatures, flow rates, CO_2 concentrations, and adsorbent loadings at atmospheric pressure. In a typical procedure, sample holders with a 10 mm diameter were filled with 0.1 g of adsorbent and glass wool was used to pack the top and bottom of the reactor containing the sample. Prior to CO_2 adsorption, the adsorbent was degassed at 110 °C for 1h with N_2 flow of 90 mL/min to remove moisture and impurities. Once the reactor has cooled down to 30 °C, a mixture of 10% CO_2 and 90% N_2 was introduced at a flow rate of 30 mL/min [23].

The CO_2 concentration of the output gas was measured using a Quantek Model 902D Carbon Dioxide Analyzer, with a computer attached for online data logging and transmission. Data recording was performed using an Onset HOBO U12 data recorder, with the HOBOware software checking CO_2 levels online every 10 s. Breakthrough curves were generated from the collected data. This experiment was repeated under varying conditions, including gas flow rates (30 to 70 mL/min), CO_2 concentrations (10% to 20%), temperatures (30 to 70 °C), and adsorbent loadings (0.1 to 1.0 g), with changes in gas volume to calculate CO_2 uptake. The experiment was replicated three times and the mean value is determined. The stability of the adsorbent was assessed by monitoring changes in its adsorption capacity over time. For the cyclic performance testing, the adsorbent was degassed at 110 °C for 1h under vacuum after each cycle.

CO_2 adsorption capacity was determined using the following Equation (1):

$$q_t = \frac{F}{m} \int_0^t (C_0 - C_t) dt \times \frac{1}{60} \quad (1)$$

where q_t is the adsorption capacity of CO_2 (mmol/g), F is the flow rate of the gaseous mixture (mL/min), t is the adsorption time (s), m is the adsorbent weight (g), while C_0 and C_t refer to the inlet and outlet CO_2 content (vol.%), respectively.

The sample that exhibited the highest CO_2 adsorption efficiency was selected for the regeneration study. To desorb CO_2 molecules from the surface of Ti-SBA-15 after completing the initial adsorption cycle and at the conclusion of the adsorption process, the adsorption column containing the adsorbent was heated to 110 °C for 1h under N_2 gas flow. Subsequently, a second cycle of CO_2 adsorption was conducted, followed by the same desorption process for a final cycle of adsorption-desorption. During the reusability test, column conditions, including an adsorption temperature of

30 °C, 10% CO_2 concentration in the feed (balanced with 90% N_2), a total feed flow rate of 30 mL/min, and 0.1 g of adsorbent remained constant. The concentration of the outlet gas was measured and recorded. This procedure was repeated for three cycles to assess the reusability of the adsorbent [23].

Results and Discussion

The experimental findings of this study are discussed and presented in this section. The characterization of the synthesized adsorbents and their adsorption performance under different process parameters is concisely explained. The reusability of the adsorbents, as well as the fixed-bed modelling and thermodynamic modelling are also briefly discussed in this section.

Characterization of adsorbents

High magnification SEM with a range of 6× to 1,000,000× was employed to examine the morphology of the synthesized adsorbents. The SEM images for the Ti-SBA-15 show a rod-like shape with uniform rod length, as seen in Figure 3. The SEM analysis illustrated the close resemblance between the shapes of titanium-functionalized SBA-15 and pure SBA-15. These structures also closely resembled Ti-SBA-15 samples synthesized by other researchers [16,24,25]. Different TIP to SBA-15 ratios during synthesis were used to achieve an optimal ratio, which could prevent intra-growth of TiO_2 and maintain the rope-like morphology without significant distortions [26].

The elemental analysis of Ti-SBA-15 was conducted using energy dispersive X-ray spectroscopy (EDX). By concentrating on a few specific regions, the elemental constitution of the Ti-SBA-15 was analyzed. The EDX spectrum for the Ti-SBA-15 is shown in the Figure 3. The EDX analysis has validated the presence of titanium (Ti), silica (Si), and oxygen (O) in the Ti-SBA-15 sample. The presence of Ti elements on the surface of the modified SBA-15 also indicated that the modification was completed effectively. Titanium is a Lewis acid that can interact with the electron-rich sites on CO_2 molecules, which are a Lewis base. This interaction is a form of chemisorption, whereby the electrons are shared or transferred between the adsorbent (Ti-SBA-15) and the adsorbate (CO_2) [27].

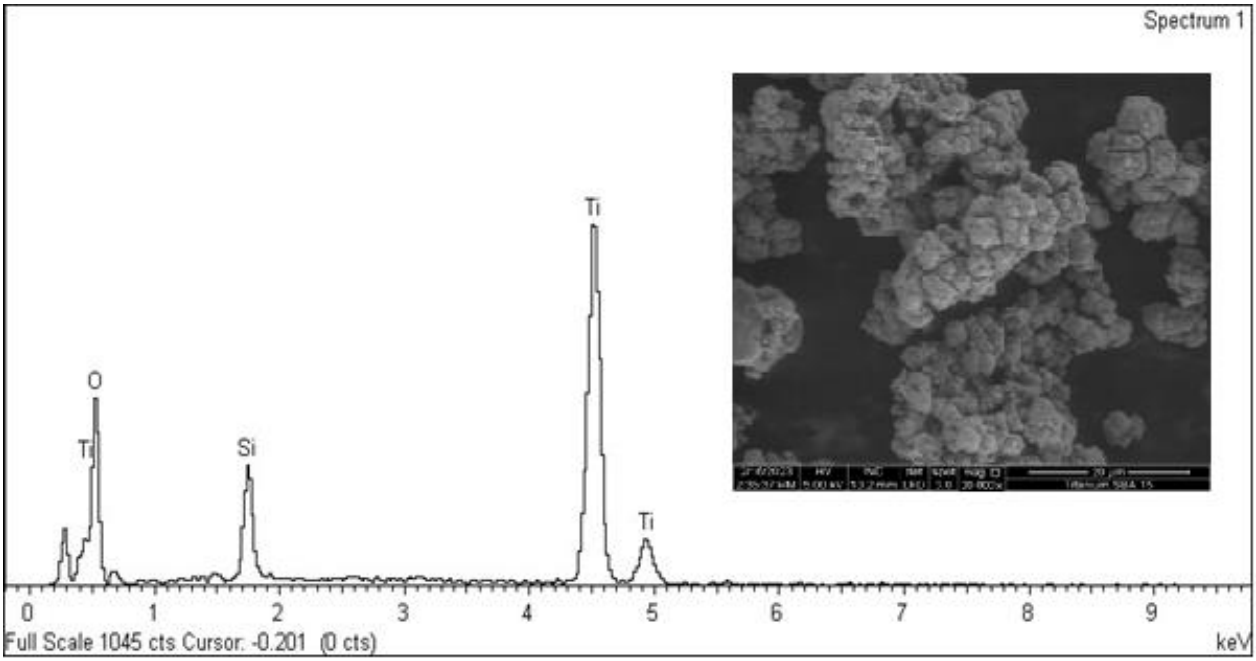

Figure 3. Scanning electron micrograph and EDX spectrum of Ti-SBA-15

TEM was employed to confirm the ordered pore structure of Ti-SBA-15. The microphotographs in Figure 4 demonstrate the adsorbent's high porosity and well-organized hexagonal array, which are particularly

evident when the electron beam is perpendicular to the adsorbent. In a parallel orientation, mesopores were observed to have a channel structure with parallel strips [28,29]. These observations supported the presence of a 2-D hexagonal long-range ordered open-framework structure, which are the characteristics of the ordered mesoporous silica, SBA-15 [30]. The structural integrity of the samples remained unaffected following their modification with TIP, which was consistent with the findings reported by other researchers. Almohammadi et al. [31] and Azimov et al. [24] similarly observed that titanium incorporation did not compromise the original pore structure of the parent SBA-15 materials.

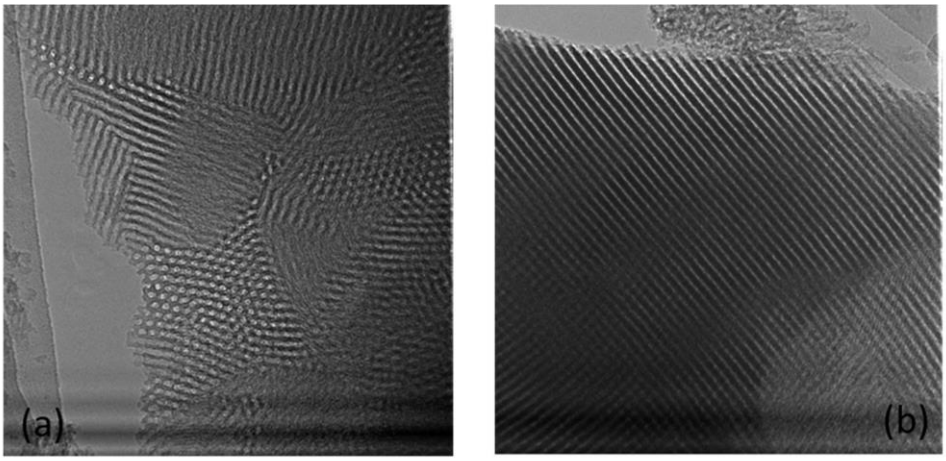

Figure 4. TEM images of pure Ti-SBA-15 in two directions: (a) perpendicular to the pore axis; and (b) parallel to the pore axis

Figure 5 illustrates the nitrogen adsorption-desorption isotherm conducted at 77 K on the synthesized adsorbent. This sample exhibited a Type IV adsorption isotherm with an H1-type hysteresis loop that indicated capillary condensation [32]. The presence of the H1 hysteresis loop implied that the synthesized Ti-SBA-15 possessed a cylindrical mesoporous and microporous structure [33]. This was a characteristic noted in various academic publications for well-formed SBA-15 [20]. However, the Ti-SBA-15 of this study demonstrated a reduced pore volume of 0.40 cm^3/g and a diminished specific surface area of 420.68 m^2/g compared to the parent SBA-15. These reductions can be attributed to the effective adherence of titanium particles to the SBA-15 surface [34]. The declines in pore volume and specific surface area were the results of the introduction of titanium into the SBA-15 structure. This modification has potentially led to the formation of titanium oxides that occupied the pores, thereby reducing the effective pore volume of this sample [17,35].

Figure 6 displays the low-angle XRD pattern for Ti-SBA-15. This well-resolved pattern showed one prominent peak and two faint peaks at 2θ corresponding to the d-spacings of (100), (110), and (200), respectively, which indicated a hexagonal symmetry with the P6mm space group [36]. The presence of these peaks is clear evidence that the SBA-15 material was successfully synthesized, as they are characteristic of its well-ordered hexagonal mesostructure with the P6mm space group [37]. The P6mm symmetry group represents a 2-D hexagonal symmetry structure that is characterized by two weak peaks (110) and (200) at 1.6° and 1.8°, respectively, which indicates the short-range ordered hexagonal amorphous structures in Ti-SBA-15 [28]. Notably, the peaks of Ti-SBA-15 shifted towards the lower angles compared to the peaks of SBA-15. This shift suggested an increase in pore diameter upon the addition of TIP to silica, which was likely due to the longer Ti-O bond compared to the Si-O bond [38].

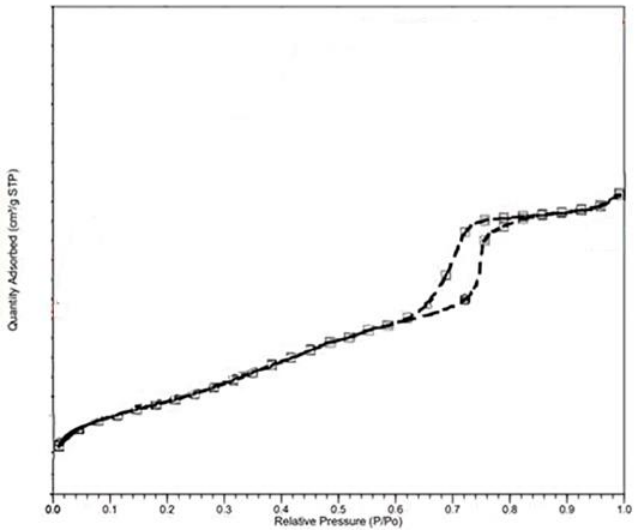

Figure 5. Nitrogen adsorption-desorption isotherm of Ti-SBA-15

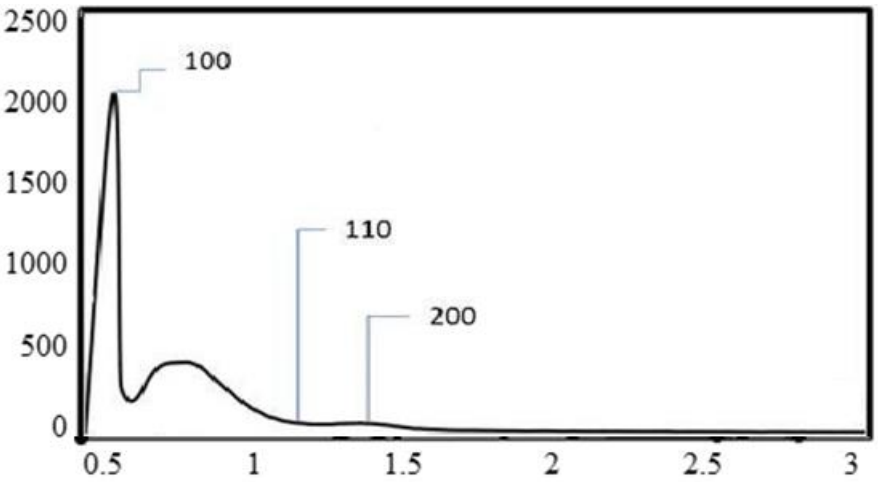

Figure 6. Low-angle XRD pattern of Ti-SBA-15

FTIR studies conducted on Ti-SBA-15 unveiled the synthesis characteristics of a highly pure product. The peaks seen at 460 cm^{-1}, 800 cm^{-1} and 1080 cm^{-1} is due to the vibration peak of the Si – O – Si bonds on the adsorbent surface [39]. The prominent broad peak at 1080 cm^{-1} (-Si-O-Si-) may be attributed to the stretching of siloxane bonds, while the peak at 460 cm^{-1} could be attributed to the bending of -Si-O-Si- bonds. Another noticeable peak may be found around 800 cm^{-1} because of the symmetric stretching of the -Si-O- bonds [37]. A rather minor peak can be observed at 1640 cm^{-1} which is directly related to the presence of adsorbed water while the broad weak band at 3480 cm^{-1} could be linked to the O-H stretching vibration of silanol groups [40]. Peaks corresponding to Ti-O-Si are evident in the FTIR spectra of the adsorbent, as seen in Figure 7(a) and (b), with the Ti-O-Si bond's vibration causing a peak at 950 cm^{-1} [41,42]. These bonds were formed when TIP interacted with the silica matrix of the adsorbent, thus providing active sites for CO_2 adsorption and offering binding sites for CO_2 molecules. Moreover, the presence of Ti-O-Si contributed to the creation of a porous structure with increased surface area, which increased the CO_2 adsorption sites. Additionally, the reactivity of these bonds promoted the activation of CO_2 molecules, which facilitated their adsorption onto the surface of the

adsorbent [43]. Both FTIR spectra also showed the presence of Ti-O bonds and -OH bonds, with an additional O=C=O bond observed in the post-adsorption spectrum, as characterized by an extra peak at 2600 cm^{-1}. The Ti-O bonds on the surface of the adsorbent can chemically interact with CO_2 molecules through coordination bonds and form stable Ti-O-CO_2 complexes. This chemisorption process can enhance the adsorption capacity of the adsorbent [44]. Furthermore, the presence of Ti-O-Si and Ti-O bonds can impart selectivity towards CO_2 adsorption over other gases due to specific interactions between CO_2 molecules and the functional groups on the adsorbent, which are crucial for efficient CO_2 capture [45].

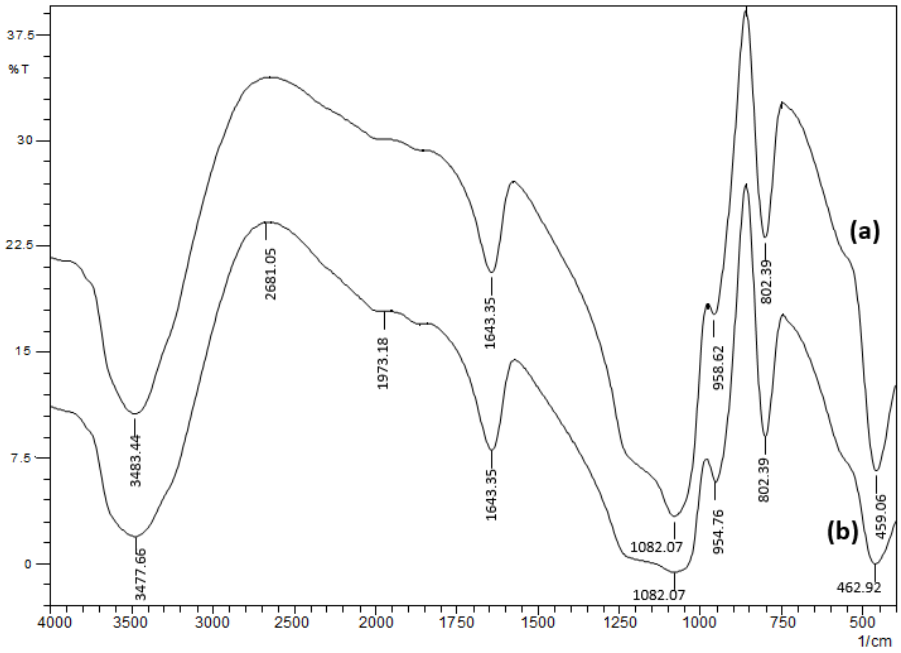

Figure 7. FTIR spectra of Ti-SBA-15: (a) before CO_2 adsorption; and (b) after CO_2 adsorption

XPS analysis was also performed to investigate the surface chemical composition and the chemical states of titanium in Ti-SBA-15. High-resolution XPS spectra of titanium 2p were acquired to further analyze the chemical states of titanium. The Ti 2p spectrum exhibited peaks at binding energies of approximately 459.0 and 464.0 eV that corresponded to Ti 2p3/2 and Ti 2p1/2, respectively, indicating the presence of titanium in the Ti(IV) oxidation state [46]. Additionally, satellite peaks were observed, suggesting the presence of titanium oxide species on the surface of Ti-SBA-15 [42]. These XPS results provided valuable insights into the surface chemistry of Ti-SBA-15 and confirmed the successful incorporation of titanium into the structure of the adsorbent.

These results are further supported by the AFM images in **Error! Reference source not found.**8(b) that show T i-SBA-15 particles in a dispersed state, with an average roughness of 1.79 nm. The surface of this sample exhibited a low root mean square (RMS) roughness, indicating minimal surface irregularities [47]. It was clear that the Ti-SBA-15 adsorbent synthesized in this study was significantly different in terms of surface topography. The peak-to-peak distance of Ti-SBA-15 was 423.42 nm with a maximum peak height of 1.29 nm. These AFM images were also consistent with the results reported by other researchers [48,49].

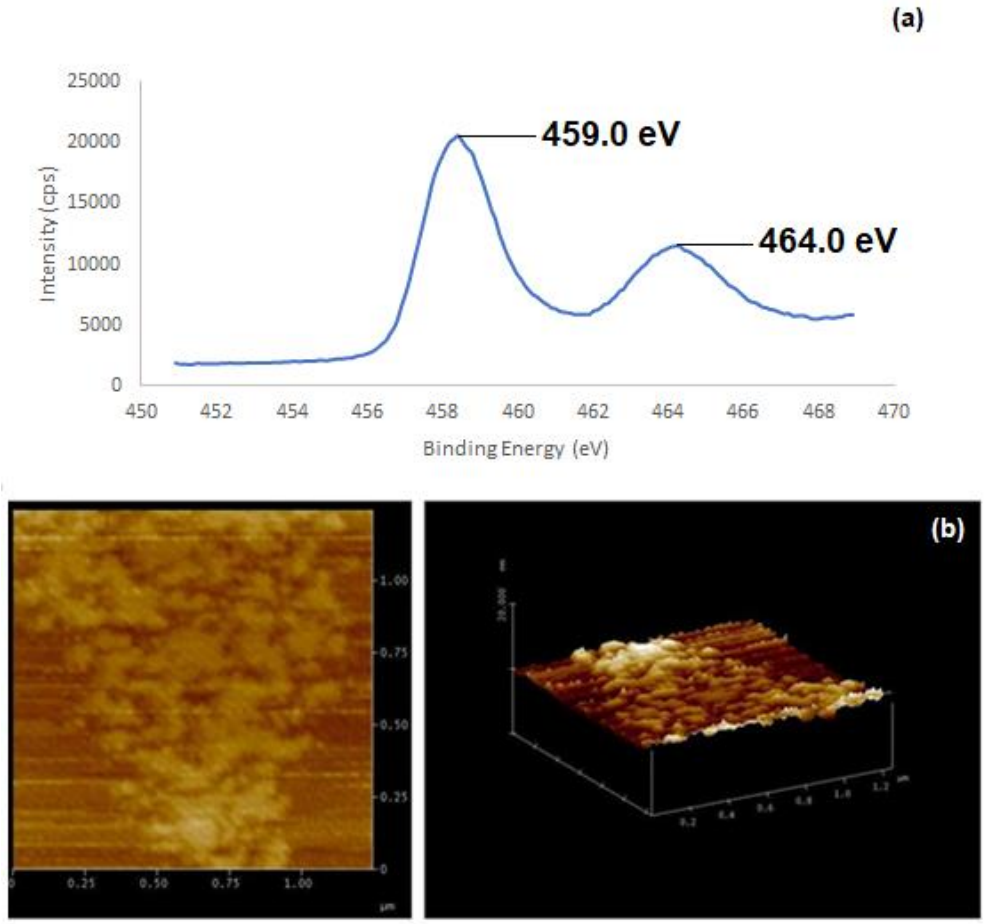

Figure 8. (a) XPS spectrum of Ti-SBA-15 (b) AFM images of Ti-SBA-15

Adsorption study

The reaction temperature, gas flow rate, CO_2 concentration and adsorbent loading were the four process parameters that were investigated in the CO_2 adsorption study using the synthesized Ti-SBA-15.

Effect of adsorption temperature

Table 1 and Figure 9 show the effect of different adsorption temperatures on CO_2 adsorption using Ti-SBA-15. The adsorption capacity of Ti-SBA-15 was 9.355, 7.523, 6.845, 6.223, and 4.890 mmol/g at 30, 40, 50, 60, and 70 °C, respectively. The adsorption capacity of Ti-SBA-15 exhibited a significantly higher increase compared to unmodified SBA-15. This could be because both physisorption and chemisorption occurred during the molecule-to-molecule interactions between CO_2 and Ti-SBA-15. When the reaction temperature was increased, the adsorption of CO_2 on Ti-SBA-15 began to decline, thus demonstrating the thermodynamic equilibrium over the whole temperature range [50]. At 70 °C, a smaller mass transfer resistance was observed compared to at 30, 40, 50, and 60 °C, as indicated by the steeper slope at this temperature. Furthermore, the breakthrough time of the adsorption process at 30 °C was substantially longer than at 40, 50, 60, and 70 °C, whereas the breakthrough curves at 50, 60, and 70 °C were relatively similar. These results showed that even though diffusion kinetics were comparable at 60 and 70 °C, they were substantially greater at 30 °C. These results were consistent with the results obtained by Sanz-Perez et al. [51]. They concluded that physical adsorbents could have a significant adsorption capacity at a lower temperature, but they would deteriorate when the temperature is increased.

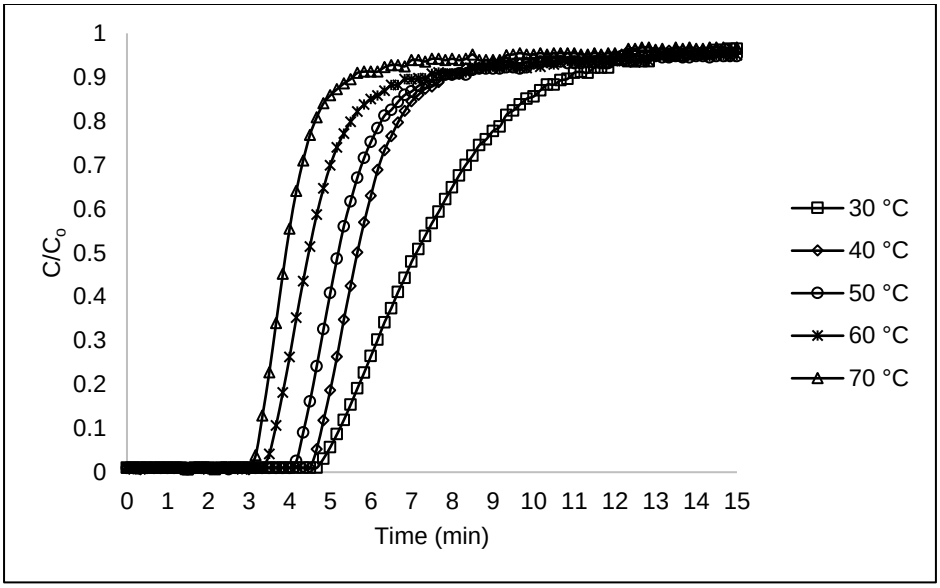

Figure 9. Breakthrough curves of Ti-SBA-15 at different adsorption temperatures

Table 1. Breakthrough times and adsorption capacities of Ti-SBA-15 at different adsorption temperatures

Adsorption Temperature (°C)	Breakthrough Time (min)	Adsorption Capacity (mmol/g)
30	4.67	9.355
40	4.50	7.522
50	4.00	6.845
60	3.33	6.223
70	3.00	4.890

Effect of gas flow rate

The investigation on how gas flow rate could affect the CO_2 adsorption performance of Ti-SBA-15 was conducted at 30, 40, 50, 60, and 70 mL/min. Figure 10 illustrates the trend of breakthrough times for Ti-SBA-15,which showed the longest time at the lowest flow rate: 30 > 40 > 50 > 60 > 70 mL/min. When the flow rate increased, the breakthrough curve began to steepen, indicating a reduced mass transfer resistance due to the higher gas flow. The results revealed a significantly shorter breakthrough time at 70 mL/min compared to at 30 mL/min. At lower flow rates, CO_2 uptake was higher because the molecules have more time to permeate the adsorbent. Conversely, at higher flow rates, the shorter contact time led to an early breakthrough because CO_2 must exit the fixed-bed column before equilibrium was reached. This phenomenon can be attributed to insufficient residence time for adsorbate permeation into the pores of the adsorbent [52]. When compared with other flow rates, the slope of the breakthrough curve at 30 mL/min appeared gentler, indicating that the lower mass transfer resistance has resulted a in narrower breakthrough width. Table 2 details the adsorption capacity and breakthrough time for the adsorbent at different flow rates. The optimal gas flow rate was identified as 30 mL/min due to the more effective interaction between the adsorbent and the adsorbate at this lower flow rate, which facilitated a prolonged contact. Although the different flow rates led to considerable reductions in adsorption capacity, the values remained consistent. Higher flow rates tended to decrease the external film mass resistance at the adsorbent's surface, thus reducing the saturation time and adsorption uptake. This observation suggests that at

higher flow rates, the external film mass resistance would be similar, resulting in breakthroughs occurring at approximately the same time and providing comparable adsorption capacities [39].

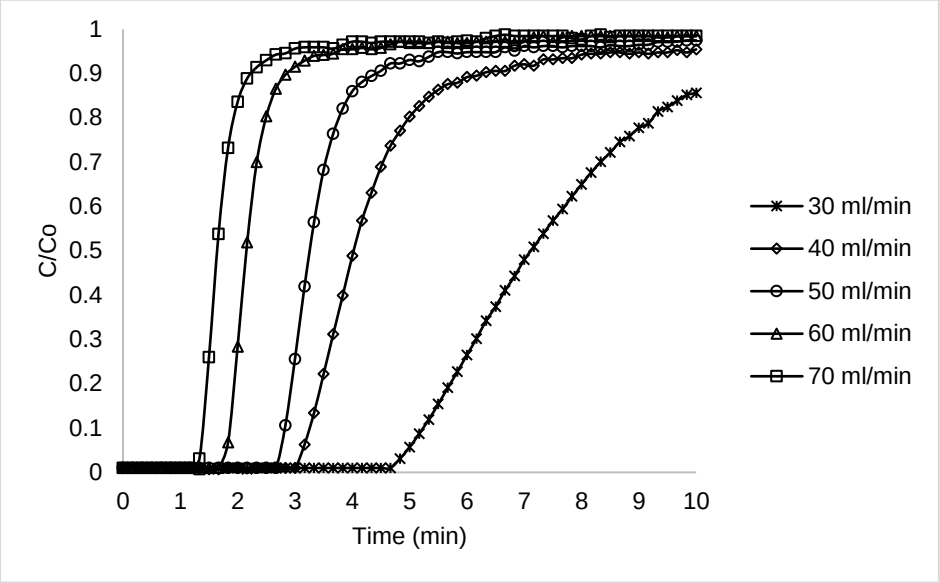

Figure 10. Breakthrough curves of Ti-SBA-15 evaluated at different CO_2 inlet flow rates

Table 2. Breakthrough times and adsorption capacities of Ti-SBA-15 at different gas flow rates

Gas Flow Rate (mL/min)	Breakthrough Time (min)	Adsorption Capacity (mmol/g)
30	4.67	9.355
40	3.00	7.644
50	2.67	7.184
60	1.67	5.793
70	1.17	5.414

Effect of CO_2 concentration

Different CO_2 concentrations were tested at 10%, 12%, 15%, 17%, and 20% to ascertain the adsorption capability of the synthesized adsorbent. These chosen concentrations are the representative of CO_2 levels found in real world applications and industrial processes [53]. The overall adsorption capacity of the adsorbent followed the trend of 20% > 17% > 15% > 12% > 10% of CO_2. Based on this trend, at lower CO_2 concentrations, the adsorption sites on the adsorbent were not fully utilized and the adsorption capacity was below the maximum. When CO_2 concentration was increased, more adsorption sites became occupied, leading to increased adsorption capacity [54]. At higher concentrations, CO_2 molecules would start to form multilayer adsorption that would occupy more spaces within the pores. This condition could have contributed to the observed increase in adsorption capacity [55]. According to Table 3, the adsorption capacity of the adsorbent is increased when CO_2 concentration is increased. Although the breakthrough times became shorter, the results demonstrated that the adsorption capacity was improved. It may be inferred that when the initial CO_2 concentration is increased, more adsorption sites are being used. This observation could be explained by the fact that at higher concentration gradients, the diffusion coefficient or mass transfer coefficient was increased, resulting in a quicker transit of the adsorbate through the adsorbents [51].

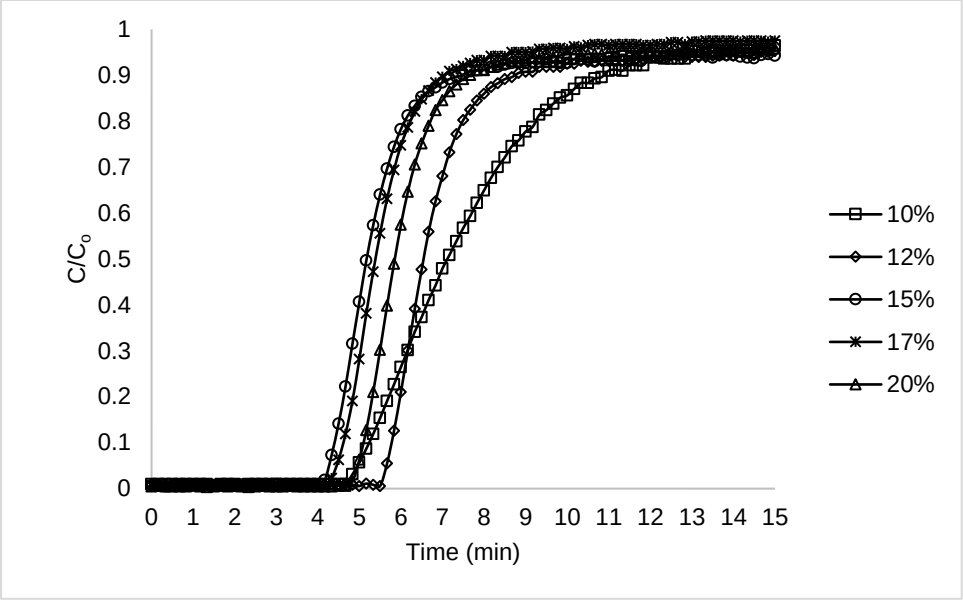

Figure 11. Breakthrough curves of Ti-SBA-15 evaluated at different CO_2 concentrations

Table 3. Breakthrough times and adsorption capacities of Ti-SBA-15 at different initial CO_2 concentrations

Initial CO_2 Concentration (%)	Breakthrough Time (min)	Adsorption Capacity (mmol/g)
10	4.67	9.355
12	5.50	10.423
15	4.00	11.107
17	4.17	13.096
20	4.67	15.507

Effect of adsorbent loading

The breakthrough curves of Ti-SBA-15 at different loadings are shown in Figure 12. The solid-gas contact area and contact duration were increased, resulting in an extension of the breakthrough time withincreased adsorbent loading. The different adsorbent loadings have greatly altered the slopes of the breakthrough curves, as illustrated in this figure. The breakthrough curves were softer when the adsorbent loading was increased, which led to a wider mass transfer zone. The variance in the slopes of the breakthrough curves can be used to explain the foundation of mass transfer. Increasing the adsorbent loading leads to an increase in bed height, which, in turn, reduces the likelihood of early saturation. The extended bed height provides more adsorbent material and active sites for CO_2 capture, allowing the adsorption process to occur over a larger volume. As a result, the adsorbate has more opportunities to interact with the adsorbent before reaching the end of the bed, effectively slowing the rate of saturation even though the flow rate remains constant [56]. Table 4 lists the adsorption capacities and breakthrough times of the adsorbent at different loadings. These results demonstrated that when the adsorbent loading was increased, its adsorption capacity would decrease, even if the breakthrough time would increase. The reason could be that some active sites were inaccessible to CO_2 molecules.

The trend for breakthrough time on different adsorbent loading could be due to variations in packing density, channeling, or void spaces within the bed. The process of packing the adsorbent bed can introduce variability, even when care is taken to replicate conditions. Small differences in how the adsorbent is packed such as

uneven density, minor channeling, or void formation can impact the flow distribution and, consequently, the breakthrough time. This irregularity in bed packing could be amplified with higher adsorbent loadings, making the trend less consistent across repeated experiments. This can cause certain regions to become saturated faster than others, leading to an earlier breakthrough in some cases and a delayed breakthrough in others. This heterogeneity can disrupt the expected linear relationship between adsorbent loading and breakthrough time [56].

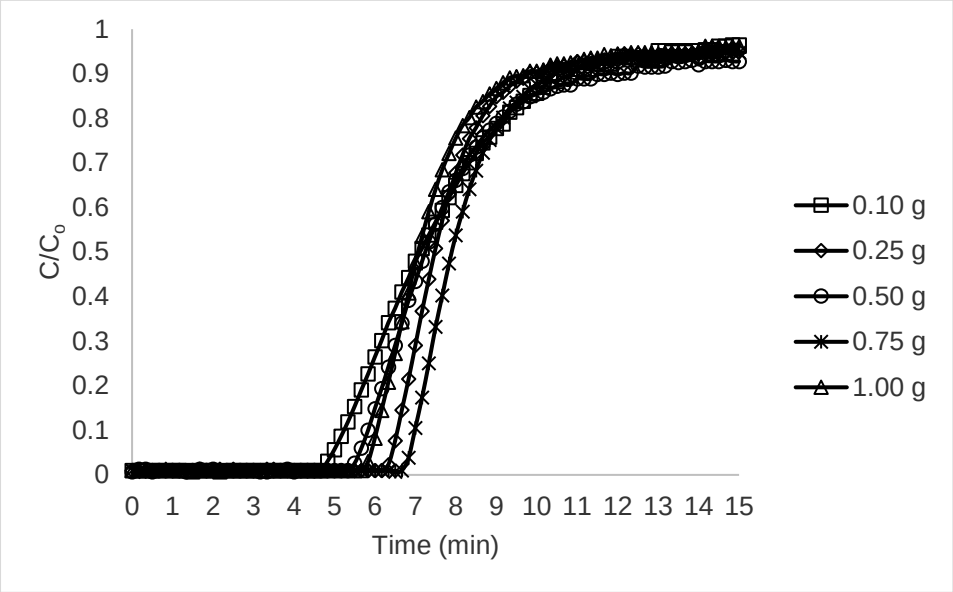

Figure 12. Breakthrough curves of Ti-SBA-15 evaluated at different adsorbent loadings

Table 4. Breakthrough time and adsorption capacity of Ti-SBA-15 at different adsorbent loadings

Adsorbent Loading (g)	Breakthrough Time (min)	Adsorption Capacity (mmol/g)
0.10	4.67	9.355
0.25	6.17	3.860
0.50	5.33	1.971
0.75	6.33	1.556
1.00	5.67	0.916

Adsorption regeneration

After the initial cycle of CO_2 adsorption, the potential for Ti-SBA-15 regeneration was investigated. To regenerate the used adsorbents, the fixed-bed reactor was heated to 110 °C for 1h, while maintaining N_2 purge at a flow rate of 90 mL/min. This study has discovered that the CO_2 molecules, which were initially adsorbed onto the Ti-SBA-15, could be completely liberated at 110 °C. Physical adsorption was the primary cause of the adsorbed CO_2 molecules' ease of desorption from Ti-SBA-15. Figure 13 illustrates the results of the three cycles of adsorption following the desorption of Ti-SBA-15. The results were adsorption capacities of 8.9 mmol/g, 7.26 mmol/g, and 6.28 mmol/g for the first, second, and third cycles, respectively. As can be observed, the adsorption capacity during the second cycle decreased by 18.4% compared to the adsorption capacity during the first cycle, while the third cycle saw a 13.5% reduction. After the first cycle, a reduction in the quantity of CO_2 adsorbed was observed, which may have been caused by insufficient CO_2 elimination during desorption. Additionally, the adsorption capacity of the

adsorbents was declining at a steady or gradual rate. This could be because the chemisorption contacts between CO_2 and the adsorbents were too strong to be broken, causing the chemisorbed CO_2 molecules to remain at the active sites [61]. The presence of CO_2 on the adsorbent surface after adsorption was proven when O=C=O bonds were present on the FTIR spectra at 2680 cm^{-1}.

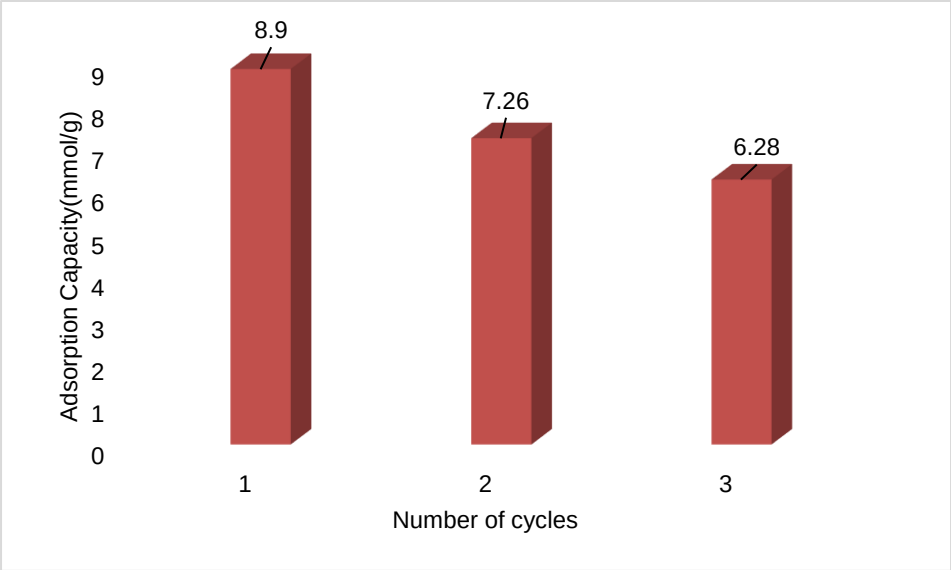

Figure 13. Adsorption capacity for cyclic CO_2 adsorption by Ti-SBA-15 (reaction conditions: gas flow rate = 30 mL/min: adsorption temperature = 30 °C: CO_2 concentration = 10%: adsorbent loading = 0.1 g)

Adsorption kinetics

The mass transfer mechanism and physio-chemical characteristics of an adsorbent can govern the rate of gas adsorption on its solid surfaces. To examine the rate of gas adsorption on porous solid adsorbent surfaces, three kinetic models are frequently utilized [62], namely the pseudo-first-order, pseudo-second-order, and Avrami models [63,64].

The pseudo-first-order model is based on optimal physical adsorption, and the positive proportionality between the adsorption rate and the number of active sites on the surface of the adsorbent. The following equation shows how this relationship can be expressed:

$$q_t = q_e[1 - exp(-k_1 t)] \quad (2)$$

where k_1 is the first order rate constant, while q_t and q_e are the quantity of CO_2 adsorbed at a particular time and at equilibrium, respectively.

The pseudo-second-order model is based on the theory of ideal chemical adsorption, and the positive proportionality between the rate of adsorption and the square of the number of active sites on the surface of the adsorbent. This model can be presented as follows:

$$q_t = \frac{k_2 q_e^2}{1 + k_2 q_e t} t \quad (3)$$

where the second order rate constant is referred to as k_2. The Avrami model, which is based on contemporaneous physical and chemical adsorption, is written as follows:

$$q_t = q_e[1 - exp(-k_a t)^{n_a}] \quad (4)$$

where the index is denoted by n_a and the kinetic rate constant is denoted by k_a.

The experimental data at different CO_2 adsorption temperatures were fitted using the pseudo-first-order, pseudo-second-order, and Avrami kinetics models. Table 5 presents the kinetics parameters for these models, alongside the experimental data and the

corresponding residual sum of squares, q%, and coefficient of regression, R^2. The analysis results showed that the Avrami model has provided a more accurate depiction of the kinetics of Ti-SBA-15 that closely aligned with the experimental data gathered during the adsorption process, as indicated by the higher R^2 values and lower q% values. Conversely, the higher values of q% for the pseudo-first-order and pseudo-second-order equations implied that the experimental CO_2 adsorption for Ti-SBA-15 did not resemble either of these two models. In the initial stages of adsorption when rapid adsorption occurred, both models tended to overestimate CO_2 adsorption. Given the favorable nature of adsorption processes involving chemical interactions as the dominant mechanism, these models exhibited significant deviation from the experimental results [65]. However, the results for the Avrami model were in good agreement with the experimental results, which indicated that physisorption could have been the primary mechanism for CO_2 adsorption onto Ti-SBA-15 [66]. Physisorption occurs as CO_2 molecules are initially attracted to the surface of Ti-SBA-15 through weak van der Waals forces [57]. The mesoporous structure of SBA-15, functionalized with titanium, provides a high surface area, facilitating the dispersion and interaction of CO_2 molecules across the adsorbent surface. As the process continues, chemisorption may occur, where CO_2 forms stronger bonds with active sites on the titanium centers. This interaction can involve the formation of carbonate or bicarbonate species, depending on the specific conditions such as temperature and CO_2 concentration. The presence of titanium enhances the affinity of the adsorbent for CO_2, potentially by providing Lewis acid sites that can interact more strongly with the electron-rich CO_2 molecules [58,59]. Additionally, the reaction temperature influences the balance between physisorption and chemisorption, with higher temperatures potentially favoring chemisorption due to the increased energy available to overcome activation barriers for bond formation [55,60].

Table 5. Kinetics Parameters of CO_2 uptake by Ti-SBA-15 at different temperatures

Kinetics models	**Temperature (°C)**				
	30	**40**	**50**	**60**	**70**
Pseudo-first-order Model					
q_e (mg/g)	2272.68	2565.64	1861.10	596.41	538.03
k_1 (min^{-1})	0.000052	0.000036	0.000053	0.00018	0.035
R^2	0.7529	0.7623	0.7964	0.8288	0.8141
Δq%	2.89	4.13	3.53	2.96	3.41
Pseudo-second-order Model					
q_e (mmol/g)	809.30	762.26	594.26	251.65	279.11
k_2 (g/mmol.min)	0.00000010	0.00000016	0.00000028	0.0000017	0.0021
R^2	0.7162	0.7621	0.7962	0.8287	0.8136
Δq%	2.88	4.13	3.54	3.00	3.42
Avrami Model					
q_e (mmol/g)	0.8257	0.7503	0.8976	0.8989	0.9268
k_A	0.000019	0.000012	0.0000018	0.000023	0.000017
n	5.4688	6.858	7.791	6.884	7.336
R^2	0.9953	0.9956	0.9953	0.9955	0.9961
Δq%	0.05	0.06	0.08	0.07	0.07

Fixed-bed adsorption column modelling

The adsorption column would have experienced axial dispersion, intraparticle diffusion resistance, and external film resistance. As a result, mathematical correlations for adsorption in fixed-bed columns must assume the presence of axial dispersion, intraparticle diffusion, external mass transfer, and non-linear isotherms [67]. The most popular mathematical models for analyzing column behavior of an adsorbate-adsorbent system are Yoon-Nelson, Bohart-Adams, and Thomas models.

The Bohart-Adams model is based on the concept that the adsorption of the adsorbate onto the adsorbent does not occur instantaneously, but rather depends on both the concentration of adsorbate in the solution and the remaining sorption capacity of the adsorbent [68]. The non-linear form of the Bohart-Adams model is expressed as follows:

$$\frac{C_t}{C_o} = exp\left[(k_{AB} \times C_o \times t) - \left(k_{AB} \times N_o \times \frac{Z}{u}\right)\right] \quad (5)$$

where Z (cm) is the height of the adsorbent bed, N_o (mg/L) is the saturation adsorption capacity per column volume, k_{AB} (L/mg.min) is the Bohart-Adams model rate constant, and u (cm/min) is the superficial velocity that can be calculated by dividing the inlet flow rate with the cross-sectional area of the fixed-bed column.

The values of k_{AB} and N_o have been determined using the non-linear regression analysis, with the corresponding constants detailed in Table 6. It was observed that the N_o value began to increase with higher CO_2 flow rates but decreased with increasing bed height. These findings underscored the influence of external mass transfer on the kinetics properties of the adsorption system during the initial stages in the fixed-bed adsorption column [69] . The Bohart-Adams model was a poor fit for the column data, which was evident from the low R^2 values and the lack of correlation between the experimental and model values.

Table 6. Parameters of the Bohart-Adams model for CO_2 adsorption on Ti-SBA-15

C_0 (%)	Flow Rate (mL/min)	Temperature (°C)	Bed Height, Z (cm)	Bohart-Adams Constant, k_{AB} (L/mg.min)	Saturation Capacity, N_o (mg/L)	R^2	Δq%
10	30	**30**	0.91	0.4944	246.55	0.9164	0.009
10	30	**40**	0.91	0.3735	234.72	0.7989	0.036
10	30	**50**	0.91	0.3342	232.37	0.7703	0.041
10	30	**60**	0.91	0.2804	228.20	0.7235	0.049
10	30	**70**	0.91	0.2422	224.14	0.6677	0.062
12	30	30	0.91	0.4739	239.92	0.8327	0.027
15	30	30	0.91	0.3349	230.46	0.7598	0.044
17	30	30	0.91	0.3520	231.14	0.7747	0.043
20	30	30	0.91	0.3960	234.48	0.7955	0.037
10	**40**	30	0.91	0.2540	297.52	0.6992	0.054
10	**50**	30	0.91	0.2025	366.14	0.6024	0.074
10	**60**	30	0.91	0.1356	436.09	0.4815	0.079
10	**70**	30	0.91	0.1105	489.63	0.4122	0.075
10	30	30	**2.27**	0.6159	100.01	0.8900	0.013
10	30	30	**4.55**	0.5289	50.40	0.9016	0.011
10	30	30	**6.83**	0.3824	31.44	0.8136	0.031
10	30	30	**9.00**	0.5426	24.61	0.8781	0.016

The Thomas model is widely used to predict the concentration profile of fixed-bed adsorption columns. This model operates under the assumption of plug flow behavior within the fixed bed and suggests that the rate-driving forces adhere to reversible kinetics of the second-order reaction. Derived from the pseudo-second-order kinetics and the Langmuir adsorption isotherm model, the Thomas model serves as a valuable tool in adsorption column analysis [69,70]. Estimates for the maximum adsorbate concentration on the adsorbent and the rate constant can be derived from the data extracted by the Thomas model. The following equation shows how the mathematical equation of the Thomas model can be articulated:

$$\frac{C_t}{C_o} = \frac{1}{1+exp\left(\left(k_{TH} \times q_o \times \frac{m}{F}\right) - (k_{TH} \times C_o \times t)\right)} \quad (6)$$

where m (g), F (mL/min), and t (min) represent the weight of the adsorbent, flow rate of CO_2 at the inlet, and total column run time, respectively. Meanwhile, k_{TH}(L/mg.min) and q_o (mg/g) correspond to the Thomas model rate constant and sorption capacity of Ti-SBA-15, respectively.

Table 7 provides a summary of the kinetics parameters, k_{TH} and q_o, derived from the non-linear regression analysis. The Thomas model was a suitable fit for the experimental data, given its lower standard deviation and higher R^2 values. With an increase in adsorbent loading, there was an observable downward trend in the q_o values. This trend could have arisen from inaccessible sorption sites on Ti-SBA-15, which led to a partial saturation of the adsorbent [71].

Table 7. Parameters of the Thomas model for CO_2 adsorption on Ti-SBA-15

C_0 (%)	Flow Rate (mL/min)	Temperature (°C)	Adsorbent Loading (g)	Thomas Constant, k_{TH} (L/mg.min)	Saturation Capacity, q_o (mg/g)	R^2	Δq%
10	30	**30**	0.10	0.6772	2811.56	0.9886	0.0012
10	30	**40**	0.10	0.0155	1826.25	0.9883	0.0021
10	30	**50**	0.10	0.0018	1298.89	0.9827	0.0031
10	30	**60**	0.10	0.9828	2299.82	0.9788	0.0037
10	30	**70**	0.10	0.0062	3257.70	0.9859	0.0026
12	30	30	0.10	1.0845	3351.58	0.9871	0.0021
15	30	30	0.10	0.0039	7216.66	0.9850	0.0028
17	30	30	0.10	0.6170	5314.32	0.9923	0.0015
20	30	30	0.10	1.4115	2481.20	0.9900	0.0018
10	**40**	30	0.10	1.6614	3810.52	0.9829	0.0031
10	**50**	30	0.10	2.0668	2652.68	0.9898	0.0019
10	**60**	30	0.10	1.3074	5038.04	0.9924	0.0012
10	**70**	30	0.10	0.0543	7269.10	0.9920	0.0010
10	30	30	**0.25**	3.2366	767.93	0.9885	0.0014
10	30	30	**0.50**	0.6117	765.23	0.9850	0.0016
10	30	30	**0.75**	0.1914	533.42	0.9843	0.0026
10	30	30	**1.00**	0.0081	374.70	0.9888	0.0015

The Yoon-Nelson model, being relatively simplistic, does not require detailed information about adsorbate characteristics, the physical properties of adsorption beds, or the type of adsorbent used. This model operates under the assumption that the probability of adsorbate breakthrough on the adsorbent correlates with the reduction in adsorption rate for each adsorbate [72,73]. The Yoon-Nelson model provides a prediction of the time taken for a breakthrough to occur in a fixed-bed column, specifically the time required to reach 50% of the breakthrough. The nonlinear equation used in the Yoon-Nelson model is as follows:

$$\frac{C_t}{C_o} = \frac{1}{\left(1+exp\left(-k_{YN}(t-\tau)\right)\right)} \quad (7)$$

where, k_{YN} (1/min) and τ (min) represent the Yoon-Nelson rate constant and the amount of time needed to attain 50% influent concentration in the effluent, respectively.

The outcomes of the non-linear regression analysis for the values of k_{YN} and τ are displayed in Table 8. The successful application of the Yoon-Nelson model in predicting the adsorption performance of Ti-SBA-15 was evident from the high R^2 values and the robust correlation between the experimental and model-generated data. The increase in k_{YN} with increasing flow rate could be attributed to a higher mass transfer force. Likewise, the decrease in τ with an increase in flow rate suggested that the fixed-bed column reached saturation more rapidly, resulting in shorter breakthrough times and quicker exhaustion of the column [74]. Furthermore, the increase in τ with increasing bed height suggested that the column became saturated progressively at

greater bed heights due to the presence of the higher loading of adsorbents [75,76].

Table 8. Parameters of Yoon-Nelson model for CO_2 adsorption on Ti-SBA-15

C_0 (%)	Flow Rate (mL/min)	Temperature (°C)	Adsorbent Loading (g)	Yoon-Nelson Constant, k_{YN} (min^{-1})	Time for 50% breakthrough, τ (min)	R^2	Δq%
10	30	**30**	0.10	2.1948	6.0449	0.9889	0.001
10	30	**40**	0.10	1.6504	5.7965	0.9883	0.002
10	30	**50**	0.10	1.5973	5.3574	0.9831	0.003
10	30	**60**	0.10	1.6298	4.6241	0.9788	0.004
10	30	**70**	0.10	2.2835	4.0069	0.9859	0.003
12	30	30	0.10	1.1549	5.6598	0.9883	0.002
15	30	30	0.10	1.8105	5.3089	0.9850	0.003
17	30	30	0.10	1.9781	5.4893	0.9923	0.001
20	30	30	0.10	1.9554	5.9632	0.9900	0.002
10	**40**	30	0.10	1.7750	4.1647	0.9845	0.003
10	**50**	30	0.10	3.2940	3.3252	0.9898	0.002
10	**60**	30	0.10	4.9652	2.1966	0.9924	0.001
10	**70**	30	0.10	5.9021	1.6802	0.9920	0.001
10	30	30	**0.25**	1.5685	7.6250	0.9885	0.001
10	30	30	**0.50**	1.4926	4.1334	0.9891	0.002
10	30	30	**0.75**	1.4354	5.9251	0.9852	0.002
10	30	30	**1.00**	1.3206	7.4728	0.9858	0.003

Thermodynamic column modelling

Table 9 presents the thermodynamic parameters concerning changes in enthalpy (ΔH), entropy (ΔS), and free Gibbs energy (ΔG) for Ti-SBA-15 at different adsorption temperatures. The process involving Ti-SBA-15 was exothermic and exhibited positive spontaneity, which were evident from the negative ΔH and ΔG values. The CO_2 adsorption onto Ti-SBA-15 was predominantly a chemical process, as indicated by the decrease in ΔG values with increasing temperature. Furthermore, the positive ΔS value signified that enthalpy increments have primarily drove the adsorption process. The slight increase in CO_2 randomness after adsorption on Ti-SBA-15 was supported by the small positive ΔS value. In this investigation, the activation energy for CO_2 adsorption was approximately -33.61 kJ/mol for Ti-SBA-15. This negative E_a value suggested that elevated adsorption temperatures did not favor CO_2 adsorption on either sample, indicating an exothermic reaction, as corroborated by the negative ΔH values from the adsorption thermodynamic analysis. The decrease in activation energy following modification could be attributed to the improved dispersion of titanium atoms, making CO_2 adsorption energetically less demanding. These thermodynamic parameters aligned with findings from other research studies [77,78,79].

Table 9. Thermodynamics parameters for Ti-SBA-15 at different temperatures

Temperature (°C)	ΔH (kJ/mol)	ΔS (kJ/mol)	ΔG (kJ/mol)
30			-32.48
40			-32.44
50	-33.61	0.0037	-32.40
60			-32.37
70			-32.33

Conclusion

Ti-SBA-15, a synthesized titanium-functionalized ordered mesoporous silica, was effectively tested for CO_2 adsorption in a fixed-bed reactor under different experimental conditions. Optimal parameters have been determined as follows: a feed flow rate of 30 mL/min, adsorbent loading of 0.1 g, CO_2 feed concentration of 10%, and adsorption temperature of 30 °C. The results showed that Ti-SBA-15 could be regenerated without significant loss of adsorption capacity, thus ensuring its reusability. The Avrami model has aptly described the kinetics of CO_2 adsorption onto Ti-SBA-15, which was mainly governed by physisorption. Both the Thomas and Yoon-Nelson models have accurately predicted CO_2 adsorption performance in the fixed-bed column, which indicated their suitability for a large-scale column design. Notably, the negative activation energy (E_a) for Ti-SBA-15 implied that higher adsorption temperatures did not hinder CO_2 uptake, thus making Ti-SBA-15 a promising adsorbent for CO_2 capture.

Acknowledgement

The authors are very thankful to Universiti Sains Malaysia for the provided facilities and support. The financial support through the Fundamental Research Grant Scheme (FRGS/1/2023/TK05/USM/02/4) is gratefully acknowledged.

References

1. IEA. (2019). CO_2 emisions from fuel combustion. *IEA Publications*, pp. 1-165.
2. Kabir, M., Habiba, U. E., Khan, W., Shah, A., Rahim, S., Rios-Escalante, P. R. D. los, Farooqi, Z. U. R., and Ali, L. (2023). Climate change due to increasing concentration of carbon dioxide and its impacts on environment in 21st century; a mini review. *Journal of King Saud University - Science*, *35*(5): 102693.
3. Shivanna, K. R. (2022). Climate change and its impact on biodiversity and human welfare. *Proceedings of the Indian National Science Academy*, 88(2): 160-171.
4. Delbeke, J., Runge-Metzger, A., Slingenberg, Y., and Werksman, J. (2019). The Paris Agreement. *Towards a Climate-Neutral Europe: Curbing the Trend*, 24-45.
5. Nasiritousi, N., and Bäckstrand, K. (2019). International climate politics in the post-Paris Era. *Nordic Economic Policy Review*, 2018: 21-50.
6. Gür, T. M. (2022). Carbon dioxide emissions, capture, storage and utilization: Review of materials, processes and technologies. *Progress in Energy and Combustion Science*, 89: 100965.
7. Lobus, N. V., Knyazeva, M. A., Popova, A. F., and Kulikovskiy, M. S. (2023). Carbon footprint reduction and climate change mitigation: A review of the approaches, technologies, and implementation challenges. *C-Journal of Carbon Research*, 9(4): 120.
8. Bhavsar, A., Hingar, D., Ostwal, S., Thakkar, I., Jadeja, S., and Shah, M. (2023). The current scope and stand of carbon capture storage and utilization ~ A comprehensive review. *Case Studies in Chemical and Environmental Engineering*, *8*(7): 100368.
9. Khandaker, T., Hossain, M. S., Dhar, P. K., Rahman, S., Hossain, A., and Ahmed, M. B. (2020). *Efficacies of Carbon-Based Adsorbents for Carbon Dioxide Capture*. pp. 1-17.
10. Ghanbari, T., Abnisa, F., and Wan Daud, W. M. A. (2020). A review on production of metal organic frameworks (MOF) for CO_2 adsorption. *Science of the Total Environment*, 707: 135090.
11. Boer, D. G., Langerak, J., and Pescarmona, P. P. (2023). Zeolites as selective adsorbents for CO_2 separation. *ACS Applied Energy Materials*, *6*(5): 2634-2656.
12. Amaraweera, S. M., Gunathilake, C. A., Gunawardene, O. H. P., Dassanayake, R. S., Cho, E. B., and Du, Y. (2023). Carbon capture using porous silica materials. *Nanomaterials*, 13(14): 2050.
13. Gkiliopoulos, D., Tsamesidis, I., Theocharidou, A., Pouroutzidou, G. K., Christodoulou, E., Stalika, E., Xanthopoulos, K., Bikiaris, D., Triantafyllidis, K., and Kontonasaki, E. (2022). SBA-15 mesoporous silica as delivery vehicle for rhbmp-2 bone morphogenic protein for dental applications. *Nanomaterials*, 12(5): 822.
14. Dziejarski, B., Serafin, J., Andersson, K., and Krzyżyńska, R. (2023). CO_2 capture materials: a review of current trends and future challenges. *Materials Today Sustainability*, 24: 100483.

15. Paulista, L. O., Ferreira, A. F. P., Castanheira, B., Đolić, M. B., Martins, R. J. E., Boaventura, R. A. R., Vilar, V. J. P., and Silva, T. F. C. V. (2024). Solar-driven thermo-photocatalytic CO_2 methanation over a structured RuO2:TiO_2/SBA-15 nanocomposite at low temperature. *Applied Catalysis B: Environmental*, 340(5): 123232.
16. Ruchomski, L., Ozimek, J., Siedliska, K., Raftopoulos, K. N., and Pielichowski, K. (2023). Characterization of Ti/SBA-15 composites synthesized by chemical vapour deposition of organic titanium compounds. *Crystals*, *13*(2): 1-15.
17. Guo, W., Hensen, E. J. M., Qi, W., Heeres, H. J., and Yue, J. (2022). Titanium phosphate grafted on mesoporous SBA-15 silica as a solid acid catalyst for the synthesis of 5-hydroxymethylfurfural from glucose. *ACS Sustainable Chemistry and Engineering*, 10(31): 10157-10168.
18. Wu, W., Bhattacharyya, K., Gray, K., and Weitz, E. (2013). Photoinduced reactions of surface-bound species on titania nanotubes and platinized titania nanotubes: An in situ FTIR study. *Journal of Physical Chemistry C*, 117(40): 20643-20655.
19. Almohammadi, G., O'Modhrain, C., Kelly, S., and Sullivan, J. A. (2020). Ti-doped SBA-15 catalysts used in phenol oxidation reactions. *ACS Omega*, *5*(1): 791-798.
20. Koh, M. H., Haji Azaman, S. A., Hameed, B. H., and Mohd Din, A. T. (2017). Surface morphology and physicochemical properties of ordered mesoporous silica SBA-15 synthesized at low temperature. *IOP Conference Series: Materials Science and Engineering*, *206*(1): 012056.
21. Li, L., Liu, D., Guo, Z., Liu, Y., and Chu, W. (2020). Improved facile synthesis of mesoporous SBA-15-CTA using citric acid under mild conditions. *Journal of Solid State Chemistry*, *282*(10): 121079.
22. Mu, Y., Huang, X., Tang, Z., and Wang, Q. (2022). Ordered mesoporous TiO2/SBA-15 confined CexWy catalysts for selective catalytic reduction of NO using NH_3. *New Journal of Chemistry*, 203(10): 1-10.
23. Ibrahim, M., Hameed, B. H., Ouakouak, A., and Mohd Din, A. T. (2022). Effect of hydrothermal carbonization parameters and performance of carbon dioxide adsorption on pineapple peel waste biochar. *Chemical Engineering and Technology*, 2022: 1-9.
24. Azimov, F., Markova, I., Stefanova, V., and Sharipov, K. (2012). Synthesis and characterization of SBA-15 AND Ti-SBA-15 nanoporous materials for DME catalysts. *Journal of the University of Chemical Technology and Metallurgy*, 47(3): 333-340.
25. Makuch, E., and Wroblewska, A. (2013). Preparation of titanium silicate Ti-SBA-15 catalyst. *Chemik*, *67*(9): 811-816.
26. Ganiyu, S. A., Ali, S. A., and Alhooshani, K. (2017). Simultaneous HDS of DBT and 4,6-DMDBT over single-pot Ti-SBA-15-NiMo catalysts: Influence of Si/Ti ratio on the structural properties, dispersion and catalytic activity. *RSC Advances*, *7*(35): 21943–21952.
27. Gao, X., Yang, S., Hu, L., Cai, S., Wu, L., and Kawi, S. (2022). Carbonaceous materials as adsorbents for CO_2 capture: synthesis and modification. *Carbon Capture Science and Technology*, 3(2): 100039.
28. Esperanza Adrover, M., Pedernera, M., Bonne, M., Lebeau, B., Bucalá, V., and Gallo, L. (2020). Synthesis and characterization of mesoporous SBA-15 and SBA-16 as carriers to improve albendazole dissolution rate. *Saudi Pharmaceutical Journal*, *28*(1): 15-24.
29. Iro, E. O. (2017). Synthesis, characterization and testing of Au / SBA-15 catalysts for elimination of volatile organic compounds by complete oxidation at low temperatures. Doctoral Thesis, Teesside University.
30. Zhai, Q. Z. (2019). Use of SBA-15 ordered nano mesoporous silica for removal of copper(II) from aqueous media: Studies on equilibrium, isotherm, kinetics and thermodynamics. *Journal of Environmental Chemical Engineering*, *7*(3): 103069.
31. Almohammadi, G., O'Modhrain, C., Kelly, S., and Sullivan, J. A. (2020). Ti-Doped SBA-15 catalysts used in phenol oxidation reactions. *ACS Omega*, *5*(1): 791-798.
32. Zhao, A., Samanta, A., Sarkar, P., and Gupta, R. (2013). Carbon dioxide adsorption on amine-impregnated mesoporous SBA-15 sorbents: Experimental and kinetics study. *Industrial and*

Engineering Chemistry Research, 52(19): 6480-6491.

33. Ullah, R., Atilhan, M., Aparicio, S., Canlier, A., and Yavuz, C. T. (2015). Insights of CO_2 adsorption performance of amine impregnated mesoporous silica (SBA-15) at wide range pressure and temperature conditions. *International Journal of Greenhouse Gas Control*, 43: 22-32.
34. Shen, J., and Hess, C. (2020). High surface area VOX/TiO_2/SBA-15 model catalysts for ammonia SCR prepared by atomic layer deposition. *Catalysts*, 10(12): 1-25.
35. Popescu, T., Oktaviani Matei, C., Culita, D. C., Maraloiu, V. A., Rostas, A. M., Diamandescu, L., Iacob, N., Savopol, T., Ilas, M. C., Feder, M., Lupu, A. R., Iacoban, A. C., Vlaicu, I. D., and Moisescu, M. G. (2022). Facile synthesis of low toxicity iron oxide/TiO2 nanocomposites with hyperthermic and photo-oxidation properties. *Scientific Reports*, 12(1) : 1-23.
36. Ma, J., Li, L., Wang, H., Du, Y., Ma, J., Zhang, X., and Wang, Z. (2022). Carbon capture and storage: History and the road ahead. *Engineering*, 14: 33-43.
37. Koh, M. H., Haji Azaman, S. A., Hameed, B. H., and Mohd Din, A. T. (2017). Surface morphology and physicochemical properties of ordered mesoporous silica SBA-15 synthesized at low temperature. *IOP Conference Series: Materials Science and Engineering*, 206(1): 012056.
38. Ye, W., Lin, Z., Dong, B., Kang, J., Zheng, X., and Wang, X. (2011). Preparation and catalytic properties of Ti-SBA-15 mesoporous materials. *Materials Sciences and Applications*, 02(06): 661-668.
39. Zhang, G., Zhao, P., Hao, L., and Xu, Y. (2018). Amine-modified SBA-15(P): A promising adsorbent for CO_2 capture. *Journal of CO_2 Utilization*, 24(10): 22-33.
40. Ullah, R., Atilhan, M., Aparicio, S., Canlier, A., and Yavuz, C. T. (2015). Insights of CO_2 adsorption performance of amine impregnated mesoporous silica (SBA-15) at wide range pressure and temperature conditions. *International Journal of Greenhouse Gas Control*, 43: 22-32.
41. Zeitler, V. A., and Brown, C. A. (1957). The infrared spectra of some Ti-O-Si, Ti-O-Ti and Si-O-Si compounds. *Journal of Physical Chemistry*, 61(9): 1174-1177.
42. Yang, L., Jiang, Z., Lai, S., Jiang, C., and Zhong, H. (2014). Synthesis of titanium containing SBA-15 and its application for photocatalytic degradation of phenol. *International Journal of Chemical Engineering*, 2014: 691562.
43. Ren, J., Li, Z., Liu, S., Xing, Y., and Xie, K. (2008). Silica-titania mixed oxides: Si-O-Ti connectivity, coordination of titanium, and surface acidic properties. *Catalysis Letters*, 124(3–4): 185-194.
44. Krischok, S., Hofft, O., and Kempter, V. (2002). The chemisorption of H_2O and CO_2 on TiO_2 surfaces: studies with MIES and UPS (HeI/II). *Surface Science*, 510: 69-73.
45. Petrovic, B., Gorbounov, M., and Masoudi Soltani, S. (2021). Influence of surface modification on selective CO_2 adsorption: A technical review on mechanisms and methods. *Microporous and Mesoporous Materials*, 312(11): 110751.
46. Larina, L. L., Omelianovych, O., Dao, V. D., Pyo, K., Lee, D., and Choi, H. S. (2021). Energy band alignment at the heterointerface between a nanostructured TiO_2 layer and Au22(SG)18clusters: Relevance to metal-cluster-sensitized solar cells. *Nanoscale*, 13(1): 175-184.
47. Rajesh Kumar, B., and Subba Rao, T. (2012). AFM studies on surface morphology, topography and texture of nanostructured zinc aluminum oxide thin films. *Digest Journal of Nanomaterials and Biostructures*, *7*(4): 1881-1889.
48. Noroozi Pesyan, N., Rezanejade Bardajee, G., Kashani, E., Mohammadi, M., and Batmani, H. (2020). Ni(II)-Schiff base/SBA-15: a nanostructure and reusable catalyst for one-pot three-component green synthesis of 3,4-dihydropyrano[3,2-c]chromene derivatives. *Research on Chemical Intermediates*, 46(1): 347-367.
49. Zauska, L., Bova, S., Benova, E., Bednarcik, J., Balaz, M., Zelenak, V., Hornebecq, V., and Almasi, M. (2021). Thermosensitive drug delivery system SBA-15-PEI for controlled release of nonsteroidal anti-inflammatory drug diclofenac sodium salt: A comparative study. *Materials*, 14(8): 1-25.
50. Bonenfant, D., Kharoune, M., Niquette, P., Mimeault, M., and Hausler, R. (2008). Advances in

principal factors influencing carbon dioxide adsorption on zeolites. *Science and Technology of Advanced Materials*, *9*(1): 013007.

51. Sanz-Pérez, E. S., Olivares-Marín, M., Arencibia, A., Sanz, R., Calleja, G., and Maroto-Valer, M. M. (2013). CO_2 adsorption performance of amino-functionalized SBA-15 under post-combustion conditions. *International Journal of Greenhouse Gas Control*, 17: 366-375.
52. Akpasi, S. O., and Isa, Y. M. (2022). Effect of operating variables on CO_2 adsorption capacity of activated carbon, kaolinite, and activated carbon – Kaolinite composite adsorbent. *Water-Energy Nexus*, 5(2022): 21-28.
53. Nwaoha, C., Supap, T., Idem, R., Saiwan, C., Tontiwachwuthikul, P., AL-Marri, M. J., and Benamor, A. (2017). Advancement and new perspectives of using formulated reactive amine blends for post-combustion carbon dioxide (CO_2) capture technologies. *Petroleum*, 3(1): 10-36.
54. Ayawei, N., Ebelegi, A. N., and Wankasi, D. (2017). Modelling and interpretation of adsorption isotherms. *Journal of Chemistry*, 2017: 3039817.
55. Gunawardene, O. H. P., Gunathilake, C. A., Vikrant, K., and Amaraweera, S. M. (2022). Carbon dioxide capture through physical and chemical adsorption using porous carbon materials: A review. *Atmosphere,* 13(3): 397.
56. Liao, P., Zhan, Z., Dai, J., Wu, X., Zhang, W., Wang, K., and Yuan, S. (2013). Adsorption of tetracycline and chloramphenicol in aqueous solutions by bamboo charcoal: A batch and fixed-bed column study. *Chemical Engineering Journal*, 228: 496-505.
57. Hu, X., Yang, X., Chen, L., Mei, M., Song, Z., Fei, Z., Dyson, P. J., and Qi, Z. (2022). Elucidating the transition between CO_2 physisorption and chemisorption in 1,2,4-triazolate ionic liquids at a molecular level. *Chemical Engineering Journal*, 435(P2): 134956.
58. Wu, W., Bhattacharyya, K., Gray, K., and Weitz, E. (2013). Role of the surface lewis acid and base sites in the adsorption of CO_2 on titania nanotubes and platinized titania nanotubes: An in-situ FT-IR study. *Journal of Physical Chemistry C*, 117(40): 20643-20655.
59. Gao, X., Yang, S., Hu, L., Cai, S., Wu, L., and Kawi, S. (2022). Carbonaceous materials as adsorbents for CO_2 capture: synthesis and modification. *Carbon Capture Science and Technology*, 3(2): 100039.
60. Gil, A. (2023). Classical and new insights into the methodology for characterizing adsorbents and metal catalysts by chemical adsorption. *Catalysis Today*, 423(12): 114016.
61. González-Barriuso, M., Gómez, L., Pesquera, C., Perdigón, A., González, F., Yedra, A., and Blanco, C. (2016). CO_2 capture at low temperature by nanoporous silica modified with amine groups. *Chemical Engineering Transactions*, *47*: 181-186.
62. Zhang, G., Zhao, P., Hao, L., and Xu, Y. (2018). Amine-modified SBA-15(P): A promising adsorbent for CO2 capture. *Journal of CO_2 Utilization*, 24(10): 22-33.
63. Ho, Y. S., and McKay, G. (1999). Pseudo-second order model for sorption processes. *Process Biochemistry*.
64. Azizian, S. (2004). Kinetic models of sorption: A theoretical analysis. *Journal of Colloid and Interface Science*, 276(1): 47-52.
65. Zhao, A., Samanta, A., Sarkar, P., and Gupta, R. (2013). Carbon dioxide adsorption on amine-impregnated mesoporous SBA-15 sorbents: Experimental and kinetics study. *Industrial and Engineering Chemistry Research*, *52*(19): 6480-6491.
66. Ibrahim, M., Hameed, B. H., Ouakouak, A., and Mohd Din, A. T. (2022). Effect of hydrothermal carbonization parameters and performance of carbon dioxide adsorption on pineapple peel waste biochar. *Chemical Engineering and Technology*, 2022: 1-9.
67. Aboelfetoh, E. F., Zain Elabedien, M. E., and Ebeid, E. Z. M. (2021). Effective treatment of industrial wastewater applying SBA-15 mesoporous silica modified with graphene oxide and hematite nanoparticles. *Journal of Environmental Chemical Engineering*, *9*(1): 104817.
68. Hayati, B., Maleki, A., Najafi, F., Gharibi, F., McKay, G., Gupta, V. K., Harikaranahalli Puttaiah, S., and Marzban, N. (2018). Heavy metal adsorption using PAMAM/CNT nanocomposite from aqueous solution in batch and continuous

fixed bed systems. *Chemical Engineering Journal*, 346(12): 258-270.

69. Rathour, R. K. S., Singh, H., Bhattacharya, J., and Mukherjee, A. (2022). Sand coated with graphene oxide-PVA matrix for aqueous Pb^{2+} adsorption: Insights from optimization and modeling of batch and continuous flow studies. *Surfaces and Interfaces*, 32(3): 102115.
70. Patel, H. (2019). Fixed-bed column adsorption study: a comprehensive review. *Applied Water Science*, *9*(3): 1-17.
71. Gong, J. L., Zhang, Y. L., Jiang, Y., Zeng, G. M., Cui, Z. H., Liu, K., Deng, C. H., Niu, Q. Y., Deng, J. H., and Huan, S. Y. (2015). Continuous adsorption of Pb(II) and methylene blue by engineered graphite oxide coated sand in fixed-bed column. *Applied Surface Science*, 330(2): 148-157.
72. Luo, J., Sun, M., Ritt, C. L., Liu, X., Pei, Y., Crittenden, J. C., and Elimelech, M. (2019). Tuning Pb(II) adsorption from aqueous solutions on ultrathin iron oxychloride (FeoCl) nanosheets. *Environmental Science and Technology*, 2019: 7027.
73. Omri, A., and Benzina, M. (2014). Almond shell activated carbon: adsorbent and catalytic support in the phenol degradation. *Environmental Monitoring and Assessment*, 186: 3875-3890.
74. Aboelfetoh, E. F., Zain Elabedien, M. E., and Ebeid, E. Z. M. (2021). Effective treatment of industrial wastewater applying SBA-15 mesoporous silica modified with graphene oxide and hematite nanoparticles. *Journal of Environmental Chemical Engineering*, *9*(1): 104817.
75. Rathour, R. K. S., Singh, H., Bhattacharya, J., and Mukherjee, A. (2022). Sand coated with graphene oxide-PVA matrix for aqueous Pb^{2+} adsorption: Insights from optimization and modeling of batch and continuous flow studies. *Surfaces and Interfaces*, 32(3): 102115.
76. Bin Jumah, M. N., Eid, M. H., AL-Huqail, A. A., Mohammad, M. A., Bin-Murdhi, N. S., Abu-Taweel, G. M., Altoom, N., Allam, A. A., and AbuKhadra, M. R. (2021). Enhanced remediation of As(V) and Hg(II) ions from aqueous environments using β-cyclodextrin/MCM-48 composite: Batch and column studies. *Journal of Water Process Engineering*, 42(5): 102118.
77. Li, X. D., and Zhai, Q. Z. (2021). Kinetics, isotherm and thermodynamic studies of S2 adsorption by (SBA-15)-Hg(II). *Water Practice and Technology*, 16(4):1475-1487.
78. Çakman, G., Ceylan, S., Topcu, Y., and Geyikçi, F. (2020). Investigation of ordered mesoporous carbon potential as CO_2 adsorbent. *Global Nest Journal*, *22*(1): 102-108.
79. Liu, Y., and Yu, X. (2018). Carbon dioxide adsorption properties and adsorption/desorption kinetics of amine-functionalized KIT-6. *Applied Energy*, 211(12): 1080-1088.